AAS 17-507

EFFECT OF SUN SHADE PERFORMANCE ON ICESAT-2 LASER REFERENCE SENSOR ALIGNMENT ESTIMATION

Chirag R. Patel*, Noah H. Smith†, Sungkoo Bae‡, and Bob E. Schutz§

Laser pointing knowledge for the Ice, Cloud, and land Elevation Satellite 2 is based on star observations from the laser reference sensor (LRS), which simultaneously observes stars and laser altimeter measurements in a single instrument coordinate frame. The LRS is modeled in this paper by two functions of the angle between star tracker zenith and the sun: pointing motion relative to the spacecraft; and sensitivity, or magnitude of the dimmest trackable star. The objective is to track thermally induced motion driven by the sun using star observations that are simultaneously degraded by the sun. Sun blinding is modeled as zero sensitivity with sunshade performance, that is the extent to which the shade prevents the sun from affecting star observations, determining the detailed sensitivity curve between sunrise and blinding. Star tracking sensitivity is relatively low due to imager issues, and sunshade issues can further reduce sensitivity in sunlight. Effects of a range of possible sensitivities and sun shades on laser pointing knowledge (and consequently geolocation of the laser spot) are characterized in this paper.

INTRODUCTION AND BACKGROUND

The Ice, Cloud, and land Elevation Satellite 2 (ICESat-2) is scheduled to launch in late 2017, and its objective is laser altimetry using the Advanced Topographic Laser Altimeter System (ATLAS) to measure ice sheet mass elevation, sea ice freeboard, land topography, and vegetation characteristics. Highly accurate measurements of the elevation at each laser footprint require a laser pointing knowledge accuracy of 1.5 arcseconds (1σ), similar to ICESat-1.

Two laser reference sensor (LRS) characteristics are significant for laser pointing knowledge: LRS sensitivity (number of trackable stars), and the nature of LRS motion relative to ATLAS. The information throughput of the LRS depends on the sensitivity of its star tracker. If the sensitivity goes to zero, the LRS outputs no information about laser pointing. When the sensitivity is low, laser pointing knowledge is dependent on knowledge of the motion of the LRS relative to the other ATLAS attitude sensors, the spacecraft star trackers (SSTs). The objective is to use LRS star observations that are degraded by the sun in order to track thermally induced motion that is driven by the sun. As the LRS line of sight approaches the sun, scattered light reduces sensitivity to star observations, while thermally induced motion increases, affecting the alignment between the star-

* Research Assistant, Center for Space Research, University of Texas, Austin, TX 78712
† Software Engineer, Voipfuture GmbH, 20097 Hamburg, Germany (contributing work performed while at Center for Space Research)
‡ Research Associate, Applied Research Laboratories, University of Texas, Austin, TX 78758
§ Professor and Associate Director, Center for Space Research, University of Texas, Austin, TX 78712 (deceased)

side and the laser-side of the LRS. The role of the LRS sunshade is to control the decrease of LRS sensitivity near the sun, that is to reduce the exposure of the LRS to the sun.

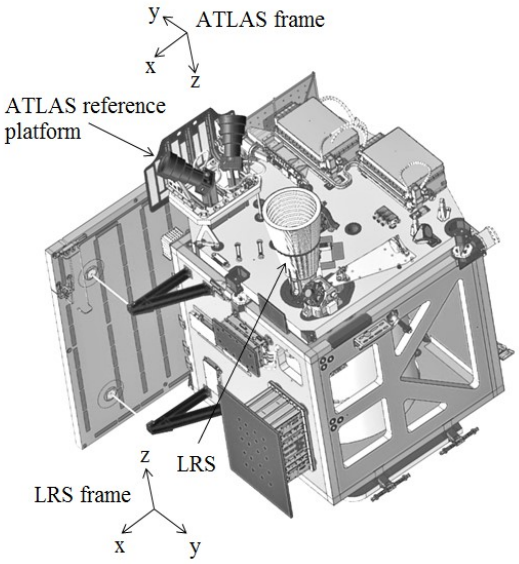

Figure 1. ATLAS and laser pointing knowledge sensors

Figure 1 shows the four pointing knowledge sensors. The LRS consists of two imagers joined back-to-back with a star tracker pointed at the zenith and a laser tracker pointed at the nadir observing the altimetry laser beams. The LRS is mounted vertically through the ATLAS optical bench and the LRS star tracker light baffle is visible. The spacecraft star trackers (SSTs) and gyro unit are mounted on a small platform attached to the ATLAS optical bench. On ICESat-1, the LRS and gyro unit were co-located and pure gyro propagation provided useful LRS alignment tracking information.[1,2] On ICESat-2, the gyro unit is located with the spacecraft star trackers on the ATLAS reference platform and significant variations are expected in the LRS to gyro unit alignment, so LRS alignment tracking concerns motion relative to the gyro unit as well as to the spacecraft star trackers.

The LRS star tracker provides two-dimensional centroid positions and brightness measurements at 10 Hz, and its field of view is $12° \times 12°$. It is capable of tracking 30 stars simultaneously. The two spacecraft star trackers output attitude estimates also at 10 Hz. The gyro unit, called the SIRU (Scalable Inertial Reference Unit), outputs angular increase measurements about each of its four sense axes (arranged in an octahedral tetrad pyramid shape) and the spacecraft records or samples these gyro measurements at 50 Hz.

Sunshade issues have arisen that are expected to have a significant negative impact on star tracker sensitivity. In particular, there have been problems with the coating applied to the vanes within the sunshade. The vanes are now expected to scatter significantly more light into the imager than was intended. This comes on top of a baseline sensitivity that is already low due to problems with the imager itself. The LRS was intended to be sensitive enough to track stars at least as dim as approximately visual magnitude 6, resulting in approximately 5,000 trackable stars with a fairly dense and uniform distribution across the sky. During testing of LRS hardware components, problems were found with the originally specified imager. The replacement imager results in a lower sensitivity of approximately visual magnitude 5.5, with about 2,500 trackable stars.

Pointing knowledge requirements are unchanged, but the LRS star observations are sparser.[3] Sunshade performance is modeled here as various sensitivity curves between sunrise (baseline sensitivity) and full blinding (zero sensitivity). The curves represent the effects of both the low baseline sensitivity and the increased scattered light from the sunshade (see Figure 5 below).

LRS MODEL

The LRS model focuses on motion and sensitivity as functions of sun angle. The orbit inclination is 92° and either the ascending or descending pass follows an approximately north-south path within 90° of the sun. The LRS-sun angle drops below 90° during every orbit. Adequate generality is provided here by studying cases with the right ascension of the sun varying between 0° and +70° relative to the right ascension of the ascending node (RAAN). The sun is encountered on the ascending pass and descending pass cases are treated as symmetric and equivalent. The ascending node is varied from right ascension 0° to 360° to encompass a diverse set of star data.

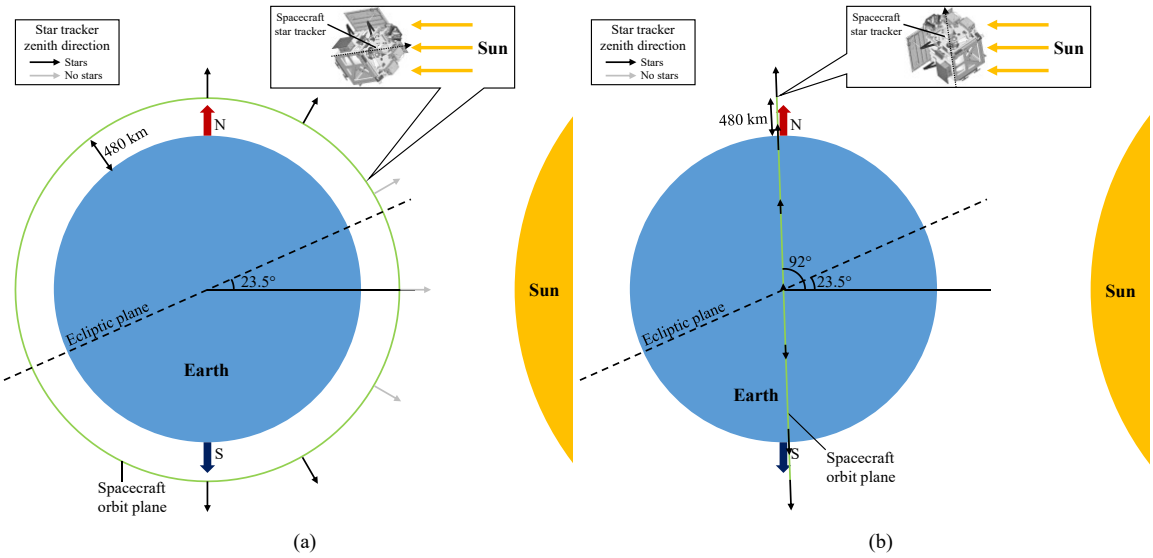

Figure 2. 92° inclination orbit configurations that showcase sun blinding (a) and no blinding (b)

With a 92° inclination, and the fact that the LRS star tracker is always pointed radially outwards in the orbit plane, it is easy to assume that the sun is hardly ever in or near the LRS star tracker field of view. However, given the inclination and semi-major axis of the orbit, and therefore the rate of change of RAAN (which is approximately 0.27°/day),[4] the sun is within 60° of the LRS star tracker zenith for approximately a third of the year for the worst case scenario described below, or a fifth of the year in the best case, making this analysis of sun blinding an important consideration, given its impact on precise pointing knowledge (see results).

The primary contribution of this paper is a characterization of pointing uncertainty over a range of possible sunshades and sensitivity curves. These two parameters are used to specify nine different curves which we believe represent a realistic range of flight data. Monte Carlo simulation is used to evaluate and compare performance for each of the nine cases.

Orbits with random sun right ascension only between 0 and 70° are considered simply because the sun has no effect on orbits for which the sun is further than 60° away from zenith. In the case where the sun passes directly through the zenith direction of the LRS star tracker (that is a sun right

ascension of 0°), the star observations are affected for up to 32 minutes out of the 94-minute orbit, considering the orbital rate of 3.75°/min.

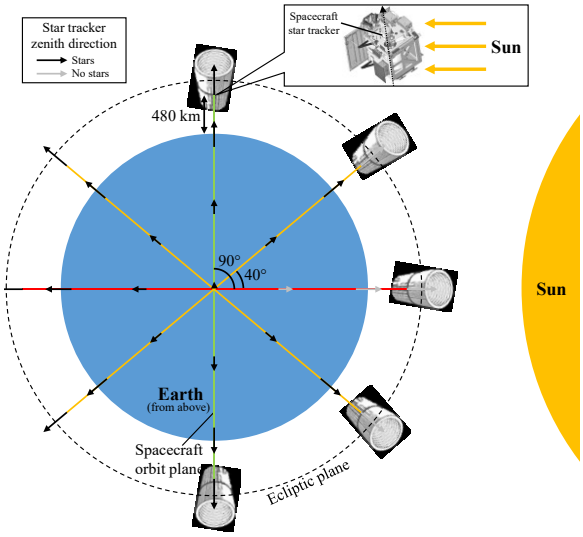

Figure 3. View from above of different orbit RAANs that show sun blinding

LRS motion is driven by the sun and normally the motion curves for roll and pitch are similar. Yaw is less significant for achieving the overall pointing and science objectives. Figure 4 shows the case of LRS motion used in this analysis. This complex model is derived from ICESat-1's alignment measurements from its Collimated Reference Source (CRS) which measured star tracker motion with respect to the optical bench that correlated with the on-orbit day/night thermal cycle (ICESat-2 has no such instrument). The roll and pitch alignments are affected differently with this once-per-orbit motion.

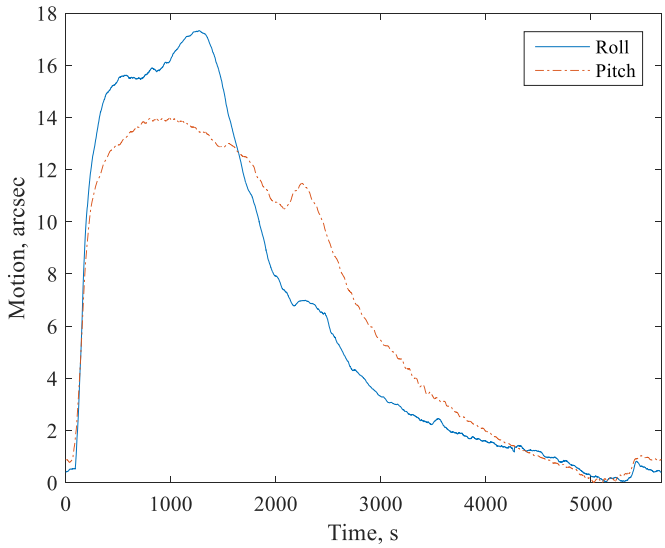

Figure 4. LRS motion from ICESat-1 CRS - roll and pitch

LRS sensitivity is progressively degraded within a ring-shaped zone surrounding the sun. The degraded zone is predicted to have inner and outer radii of approximately 20° and 50° respectively. Both radii are functions of sunshade performance, and the inner radius is strongly constrained by the size of the solar corona as well as the solar disk. The nine cases studied here are shown in Figure 5, and the three cases in color are the expected middle case and two extremes (a best case with high sensitivity and narrow degraded zone, and a worst case with low sensitivity and wide degraded zone). These three cases are examined in more detail later.

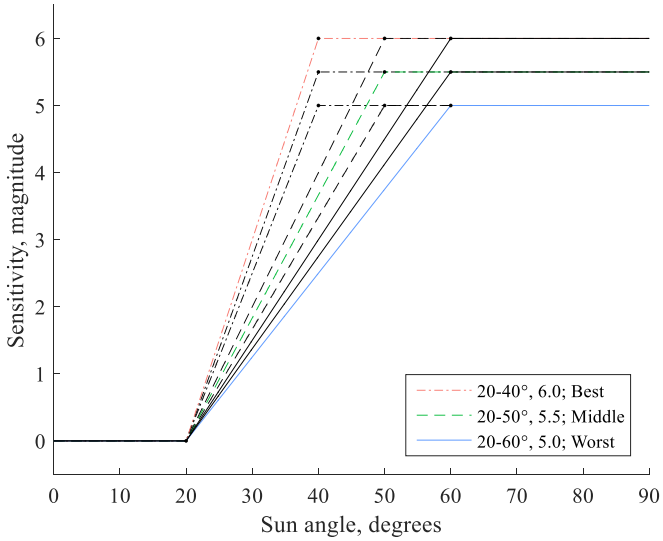

Figure 5. LRS sensitivity versus sun angle for three baseline sensitivities and three degraded zones

LRS MOTION TRACKING

The objective is to simultaneously track the ATLAS reference platform attitude and LRS alignment; in other words, the rotations from the celestial frame to the reference platform frame and from the reference platform frame to the LRS frame. The reference platform is a small bench isolated from the main optical bench on three struts and carrying the two spacecraft star trackers and gyro unit.

All spacecraft hardware is modeled here as two rigid bodies: the ATLAS reference platform, and the LRS. The performance analysis presented here is based on simulation of the rigid body model with reference platform attitude and LRS alignment being the two main outputs given an input truth. The tracking error quantities in attitude and alignment are simply the errors (differences) between estimated and true reference platform attitudes, and estimated and true LRS alignments respectively. There is also a third quantity, the LRS laser vectors, but the results given here focus on attitude and alignment tracking, assuming the ideal situation where the laser tracker to reference platform alignment is well-known.

Simulation Truth

The truth for spacecraft frame attitudes and rates used in the performance is called SIMV9 (Simulation Version 9) and is the fundamental truth dataset for all artificial telemetry and test processing in the ICESat-2 position, pointing, and geolocation knowledge group. It provides data for a 24-hour

interval that includes realistic pointing maneuvers, including ocean scans. The test case used in this paper is taken from the beginning of the SIMV9 truth data. The simulation lasts for 1 orbit (5645 seconds), and does not include the ocean scans, target scans, and around the world scan maneuvers.[3] Including those maneuvers would skew results away from the sunshade and star sensor performance vs. alignment results objective of the paper.

This truth dataset provides true attitudes and rates for $\mathbf{A}_i^{ATLAS}$ at 1 second intervals.* These are then resampled or interpolated to 0.1 second intervals to match the expected observation rates of the star tracker measurements. Measurement models are then used to introduce sensor characteristics and deterministic errors. Stochastic errors (noise) are added and characterized in terms of the error models. It is also assumed that these artificial measurements are received by the processor at the same time. In practice, the star tracker and gyro measurements may be asynchronous.

States

An alignment filter is used to simultaneously predict the measurements from all three star trackers. The measurement residuals are used to update the filter states, which include the reference platform attitude, gyro rate bias, and time-varying corrections to reference alignments. The combined states represent the attitude of the spacecraft and alignments of the star trackers. Alignment filtering has been discussed in the literature, especially since 2000 by Pittelkau.[5,6]

Time-varying rotation vectors $\mathbf{a}_{TRK}(t)$ that represent small alignment corrections to reference alignments $\mathbf{A}_{ATLAS}^{TRK}$ are included in the attitude models for the three trackers:

$$\mathbf{A}_i^{LRS}(t) = \mathbf{A}(\mathbf{a}_{LRS}(t))\mathbf{A}_{ATLAS}^{LRS}\mathbf{A}_i^{ATLAS}(t) \tag{1}$$

$$\mathbf{A}_i^{SST1}(t) = \mathbf{A}(\mathbf{a}_{SST1}(t))\mathbf{A}_{ATLAS}^{SST1}\mathbf{A}_i^{ATLAS}(t) \tag{2}$$

$$\mathbf{A}_i^{SST2}(t) = \mathbf{A}(\mathbf{a}_{SST2}(t))\mathbf{A}_{ATLAS}^{SST2}\mathbf{A}_i^{ATLAS}(t) \tag{3}$$

The attitude models above are for the simulation truth. For the equivalent models for the three star trackers' estimated attitudes:

$$\mathbf{A}_i^{LRS}(t) = \mathbf{A}(\mathbf{a}_{LRS}(t))\mathbf{A}_b^{LRS}\mathbf{A}_i^{b}(t) \tag{4}$$

$$\mathbf{A}_i^{SST1}(t) = \mathbf{A}(\mathbf{a}_{SST1}(t))\mathbf{A}_b^{SST1}\mathbf{A}_i^{b}(t) \tag{5}$$

$$\mathbf{A}_i^{SST2}(t) = \mathbf{A}(\mathbf{a}_{SST2}(t))\mathbf{A}_b^{SST2}\mathbf{A}_i^{b}(t) \tag{6}$$

The state vector is

$$\mathbf{x}(t) = \begin{bmatrix} \mathbf{a}(t)^T & \mathbf{b}(t)^T & \mathbf{a}_{LRS}(t)^T & \mathbf{a}_{SST1}(t)^T & \mathbf{a}_{SST2}(t)^T \end{bmatrix}^T \tag{7}$$

where $\mathbf{a}(t)$ is the attitude error and $\mathbf{b}(t)$ is the gyro rate bias. The $\mathbf{a}_{TRK}(t)$ are time-varying rotation vectors that represent small alignment corrections to the reference alignments between the tracker and the ATLAS reference platform, and the results will focus on the most relevant $\mathbf{a}_{LRS}(t)^T$

* A section on mathematical notation is provided after the conclusions

term. These states are estimated using a filter based on the standard attitude filter called the Multiplicative Extended Kalman Filter.[7]

The three filter phases (state propagation using rate observations, attitude update using simulated attitude observations, and alignment update using simulated star observations) are described in the following sections.

The covariance matrix $\mathbf{P}$ is given by

$$\mathbf{P}_{15\times15} \equiv E\{(\mathbf{x}-\hat{\mathbf{x}})(\mathbf{x}-\hat{\mathbf{x}})^T\} = \begin{bmatrix} \mathbf{P_a} & \mathbf{P_{ab}} & & & & \\ \mathbf{P_{ab}} & \mathbf{P_b} & & & & \\ & & \mathbf{P}_{LRS} & & & \\ & & & \mathbf{P}_{SST1} & & \\ & & & & \mathbf{P}_{SST2} & \end{bmatrix} \tag{8}$$

where $\mathbf{P}$ is partitioned into 3×3 attitude $\mathbf{P_a}$, rate $\mathbf{P_b}$, correlation $\mathbf{P_{ab}}$, and alignment $\mathbf{P}_{TRK}$ sub-matrices. By linearizing the continuous-time state equation, we get

$$\begin{bmatrix} \dot{\boldsymbol{\delta}} & [\boldsymbol{\omega}_{ref}\times] & \mathbf{I}_{3\times3} & & & & \\ \dot{\boldsymbol{\delta}} & \mathbf{0}_{3\times3} & \mathbf{0}_{3\times3} & & & & \\ \dot{\boldsymbol{\delta}} & & & \mathbf{0}_{3\times3} & & & \\ \dot{\boldsymbol{\delta}} & & & & \mathbf{0}_{3\times3} & & \\ \dot{\boldsymbol{\delta}} & & & & & \mathbf{0}_{3\times3} & \end{bmatrix} \begin{bmatrix} \boldsymbol{\delta a} \\ \boldsymbol{\delta b} \\ \boldsymbol{\delta a}_{LRS} \\ \boldsymbol{\delta a}_{SST1} \\ \boldsymbol{\delta a}_{SST2} \end{bmatrix} + \mathbf{I}_{15\times15} \begin{bmatrix} \boldsymbol{\eta}_{ARW} \\ \boldsymbol{\eta}_{RRW} \\ \boldsymbol{\eta}_{LRS} \\ \boldsymbol{\eta}_{SST1} \\ \boldsymbol{\eta}_{SST2} \end{bmatrix} \tag{9}$$

where the gyro rate bias $\boldsymbol{\delta b}$ and alignments $\boldsymbol{\delta a}_{LRS}$, $\boldsymbol{\delta a}_{SST1}$, and $\boldsymbol{\delta a}_{SST2}$ are driven only by process noise. The discrete-time process noise matrix is given by

$$\mathbf{Q}_k(t) = \begin{bmatrix} (\sigma_{AWN}^2 + t\sigma_{ARW}^2 + (t^3/3)\sigma_{RRW}^2)\mathbf{I} & (t^2/2)\sigma_{RRW}^2\mathbf{I} & & & & \\ (t^2/2)\sigma_{RRW}^2\mathbf{I} & t\sigma_{RRW}^2\mathbf{I} & & & & \\ & & t\sigma_{LRS}^2\mathbf{I} & & & \\ & & & t\sigma_{SST1}^2\mathbf{I} & & \\ & & & & t\sigma_{SST2}^2\mathbf{I} & \end{bmatrix} \tag{10}$$

Propagation

Gyro observations represent changes in attitude over time, and gyro unit rate observations are simulated by adding measurement noise to the true attitude rate $\boldsymbol{\omega}_k$, producing an observed rate $\boldsymbol{\omega}_{g,k}$. The model used in these simulations is $\boldsymbol{\omega}_{g,k} = \boldsymbol{\omega}_k + \mathbf{b}_k + \boldsymbol{\eta}_{awn}$ where $\boldsymbol{\eta}_{awn}$ is short-term angular white noise in the gyro output with variance $E\left\{\boldsymbol{\eta}_{awn}\boldsymbol{\eta}_{awn}^T\right\} = \sigma_{awn}^2\mathbf{I}$. To simulate random walk, random values $\Delta\mathbf{b}_k$ are added to the rate bias every time step, $\mathbf{b}_k = \mathbf{b}_{k-1} + \Delta\mathbf{b}_k$ with variance $E\left\{\Delta\mathbf{b}_k\Delta\mathbf{b}_k^T\right\} = \sigma_{\Delta\mathbf{b}}^2\mathbf{I}$. Angular white noise σ_{awn} is one of the three kinds of uncertainties quantified here. The other two are angular random walk σ_{arw}, and rate random walk σ_{rrw}. Uncertainties for the ICESat-2 SSIRU gyro unit are given by Northrop Grumman as

$\sigma_{awn} = 1.5331\times10^{-8}\,\text{rad/Hz}^{1/2}$, $\sigma_{arw} = 1.7453\times10^{-8}\,\text{rad/s}^{1/2}$, $\sigma_{rrw} = 2.424\times10^{-11}\,\text{rad/s}^{3/2}$, and $\sigma_{\Delta\mathbf{b}} = 7.6\times10^{-12}\,\text{rad/s}$.*

For the filter state propagation step, rate observations $\boldsymbol{\omega}_g$ are used, which come from time-tagged angular changes output by the SSIRU gyro unit. The gyro noises are added to these measurements to come up with the filter model for the angular rate: $\boldsymbol{\omega} = \boldsymbol{\omega}_g + \mathbf{b} + \boldsymbol{\eta}_{arw}$ where $d\mathbf{b}/dt = \boldsymbol{\eta}_{rrw}$. Assuming that the attitude rate $\boldsymbol{\omega}_g$ is approximately constant for each filter time step, the attitude prediction for the next time step can be calculated using the rotation vector $\mathbf{a} = \Delta t\left(\boldsymbol{\omega}_g + \mathbf{b}\right)$. The state transition matrix for covariance and state propagation is

$$\Phi_k(t) = \begin{bmatrix} \mathbf{R}(\mathbf{a}_p) & \mathbf{S}(\mathbf{a}_p) & & & & \\ \mathbf{0}_{3\times3} & \mathbf{I}_{3\times3} & & & & \\ & & \mathbf{I}_{3\times3} & & & \\ & & & \mathbf{I}_{3\times3} & & \\ & & & & \mathbf{I}_{3\times3} & \end{bmatrix} \tag{11}$$

$$\mathbf{R}(\mathbf{a}) = (\cos a)\mathbf{I} - \left(\frac{\sin a}{a}\right)[\mathbf{a}\times] + \left(\frac{1-\cos a}{a^2}\right)\mathbf{a}\mathbf{a}^T \tag{12}$$

$$\mathbf{S}(\mathbf{a}) = t\left[\left(\frac{\sin a}{a}\right)\mathbf{I} - \left(\frac{1-\cos a}{a^2}\right)[\mathbf{a}\times] + \left(\frac{a-\sin a}{a^3}\right)\mathbf{a}\mathbf{a}^T\right] \tag{13}$$

After the propagation step, the attitude estimate is $\mathbf{q}_{b,k+1} = \mathbf{q}\left(\mathbf{a}_p\right)\otimes\mathbf{q}_{b,k}$, the state estimate is $\mathbf{x}_{k+1} = \mathbf{x}_k$, and the covariance is $\mathbf{P}_{k+1} = \boldsymbol{\Phi}_k\mathbf{P}_k\boldsymbol{\Phi}_k^T + \mathbf{Q}_k$.

Attitude Update

The estimated attitude is corrected using the quaternion observations output by the spacecraft star trackers, with observation errors modeled as Gaussian white noise and added to the quaternions output by the SSTs. The observations from SST1 (the SST2 case is the same) used in the filter are modeled as $\mathbf{q}_i^{SST1} = \mathbf{q}\left(\boldsymbol{\eta}_{SST}\right)\otimes\mathbf{q}_{ATLAS}^{SST1}\otimes\mathbf{q}_i^{ATLAS}$ where $\boldsymbol{\eta}_{SST}$ is a rotation vector that gives the observation uncertainty matrix $\mathbf{R} = E\left\{\boldsymbol{\eta}_{SST}\boldsymbol{\eta}_{SST}^T\right\} = \text{diag}\left(\left[\sigma_{SSTx}^2 \quad \sigma_{SSTy}^2 \quad \sigma_{SSTz}^2\right]\right)$, and $\mathbf{q}_{ATLAS}^{SST1}$ is the reference alignment for SST1. The manufacturer specifications for observation uncertainties from the SSTs are $\sigma_{SSTx} = \sigma_{SSTy} = 1.5\,\text{arcsec}$ and $\sigma_{SSTz} = 12.2\,\text{arcsec}$.

The predicted SST1 attitude from the filter is $\mathbf{q}_{ATLAS}^{SST1}\otimes\mathbf{q}_i^b$ and the observation residual $\Delta\mathbf{y}$ is $\left[\Delta\mathbf{y}^T/2 \quad q_4\right]^T = \mathbf{q}_i^{SST1}\otimes\left(\mathbf{q}_{ATLAS}^{SST1}\otimes\mathbf{q}_i^b\right)^*$. The usual EKF steps are performed to update the attitude using the observation sensitivity matrix $\mathbf{H} = \left[\mathbf{A}_{ATLAS}^{SST1} \quad 0 \quad 0 \quad 0 \quad 0\right]$, Kalman gain

* "Scalable SIRU Family", Northrup Grumman, http://www.northropgrumman.com/Capabilities/SIRU/Documents/Scalable_SIRU_Family.pdf

$\mathbf{K} = \mathbf{P}\mathbf{H}^T\left(\mathbf{H}\mathbf{P}\mathbf{H}^T + \mathbf{R}\right)^{-1}$, estimated state correction $\Delta\mathbf{x} = \begin{bmatrix}\Delta\mathbf{a}^T & \Delta\mathbf{b}^T & \Delta\mathbf{a}_{LRS}^T & \Delta\mathbf{a}_{SST1}^T & \Delta\mathbf{a}_{SST2}^T\end{bmatrix}^T = \mathbf{K}\Delta\mathbf{y}$, and covariance $\mathbf{P}_+ = \left(\mathbf{I} - \mathbf{K}\mathbf{H}\right)\mathbf{P}_-$. From these updated states, the new gyro rate bias is $\mathbf{b}_+ = \mathbf{b}_- + \Delta\mathbf{b}$ and finally the updated attitude estimate is $\mathbf{q}_{b+} = \mathbf{q}\left(\Delta\mathbf{a}\right) \otimes \mathbf{q}_{b-}$. This process is performed again for observations from the second spacecraft star tracker, SST2.

Star Tracker Sensitivity

Alignment tracking errors are primarily due to observation errors in tracking stars, which is where the information for LRS alignment comes from. LRS alignment is tracked and updated only when star observations are available, so if the LRS star tracker is unable to track stars dim enough to cover the whole sky, alignment tracking suffers when there are no star observations. Star observations will also disappear when the sun is near the spacecraft zenith, near the boresight direction of the LRS star tracker.

LRS sensitivity is characterized by the maximum instrument magnitude of a star observable by the LRS star tracker. Instrument and astronomical magnitudes can be related by the equation

$$m - m_{\text{ref}} = -2.5\log_{10}\left(i / i_{\text{ref}}\right) \tag{14}$$

where m_{ref} and i_{ref} are reference magnitude and intensity of the star's spectral input power. The estimated instrument sensitivity for the LRS is 5.5; that is, the LRS star tracker will not observe stars that are dimmer than instrument magnitude 5.5. For comparison purposes, and to see the effects of lower- or higher-than-expected sensor sensitivity, the three cases studied in this paper are LRS sensitivities 5.0, 5.5, and 6.0.

Two other sources of error are deterministic errors and noise in the star observations. Deterministic errors such as distortion are corrected within the processor.[8] The effects of noise are reduced by observing more stars n, because uncertainty scales with $1/\sqrt{n}$. Low star sensor sensitivity results in fewer star observations and therefore larger uncertainties.

Another source of alignment tracking errors are the characteristics of the alignment variations. If the alignment variations are especially sudden, tracking errors are expected to be larger, even more so when there are simultaneously no star observations. In this study, Monte Carlo simulations are run for a complex case of alignment variation where the true variation is derived from ICESat-1 flight data (see Figure 4).

Alignment Update

Star observations for LRS alignment tracking can be simulated using the true LRS attitude $\mathbf{A}_i^{LRS}(t)$, star catalog unit vectors $\mathbf{u}'$ in the celestial frame, and measurement noise $\boldsymbol{\eta}$ with covariance $\mathbf{R} = E\{\boldsymbol{\eta}\boldsymbol{\eta}^T\} = \sigma_{obs}^2\mathbf{I}_{2\times 2}$ as

$$\mathbf{y} = \mathbf{h}(\mathbf{u}_{obs}) = \mathbf{h}(\mathbf{A}_i^{LRS}\mathbf{u}') + \boldsymbol{\eta} \tag{15}$$

Where $\mathbf{h}(\mathbf{u}) \equiv \begin{bmatrix}h & v\end{bmatrix}^T \equiv \begin{bmatrix}u_1/u_3 & u_2/u_3\end{bmatrix}^T$ are the observations in the star tracker field of view in the h, v coordinate plane.

Observation residuals are $\Delta\mathbf{y} = \mathbf{h}(\mathbf{u}_{obs}) - \mathbf{h}(\hat{\mathbf{A}}_i^{LRS}\mathbf{u}')$ where $\hat{\mathbf{A}}_i^{LRS}$ is the estimated LRS attitude. The star observations and filter states are related through the sensitivity matrix $\mathbf{H}$ where

$$\mathbf{H} = \frac{\partial \mathbf{y}}{\partial \mathbf{x}} = \frac{\partial \mathbf{h}}{\partial \mathbf{u}}\frac{\partial \mathbf{u}}{\partial \mathbf{x}} = \frac{\partial \mathbf{h}}{\partial \mathbf{u}}\left[\frac{\partial \mathbf{u}}{\partial \mathbf{a}} \quad 0 \quad \frac{\partial \mathbf{u}}{\partial \mathbf{a}_{LRS}} \quad \frac{\partial \mathbf{u}}{\partial \mathbf{a}_{SST1}} \quad \frac{\partial \mathbf{u}}{\partial \mathbf{a}_{SST2}}\right] \tag{16}$$

$$\frac{\partial \mathbf{h}}{\partial \mathbf{u}} = \begin{bmatrix} 1/u_3 & 0 & -u_1/u_3^2 \\ 0 & 1/u_3 & -u_2/u_3^2 \end{bmatrix} \tag{17}$$

Where the sensitivity of observed star unit vectors to body frame attitude and sensor alignment variations are represented by $\partial\mathbf{u}/\partial\mathbf{a}$ and $\partial\mathbf{u}/\partial\mathbf{a}_j$ respectively, and they are derived using[5,6] as follows.

For $\partial\mathbf{u}/\partial\mathbf{a}$ the j^{th} alignment is held constant and absorbed in $\mathbf{A}_b^j$. For a reference attitude $\mathbf{A}_i^r(t)$ close to $\mathbf{A}_i^b(t)$ with the approximation $\mathbf{A}(\mathbf{a}) \approx (\mathbf{I} - [\mathbf{a}\times])$ for a small attitude error $\mathbf{a}$, the total attitude is modeled as $\mathbf{A}_i^b(t) = \left(\mathbf{I} - \left[\mathbf{a}\times\right]\right)\mathbf{A}_i^r(t)$. Observed and reference unit vectors are related by $\mathbf{u} = \mathbf{A}_b^j\mathbf{A}_i^b(t)\mathbf{u}'$ and substituting

$$\mathbf{u} = \mathbf{A}_b^j\mathbf{A}_i^r(t)\mathbf{u}' - \mathbf{A}_b^j\left[\mathbf{a}\times\right]\mathbf{A}_i^r(t)\mathbf{u}' \tag{18}$$

$$\mathbf{u} = \mathbf{A}_b^j\mathbf{A}_i^r(t)\mathbf{u}' + \mathbf{A}_b^j\left[\mathbf{A}_i^r(t)\mathbf{u}'\times\right]\mathbf{a} \tag{19}$$

$$\partial\mathbf{u}/\partial\mathbf{a}_j = \mathbf{A}_b^j\left[\mathbf{A}_i^b(t)\mathbf{u}'\times\right] \tag{20}$$

for $\mathbf{a}_i^r \to \mathbf{a}_i^b$ as $\mathbf{a} \to \mathbf{0}$.

For $\partial\mathbf{u}/\partial\mathbf{a}_j$ with a reference alignment $\mathbf{A}_b^r$ close to $\mathbf{A}_b^j$ and the similar approximation $\mathbf{A}(\mathbf{a}_j) \approx (\mathbf{I} - [\mathbf{a}_j\times])$, the jth sensor alignment is modeled as $\mathbf{A}(\mathbf{a}_j)\mathbf{A}_b^r = (\mathbf{I} - [\mathbf{a}_j\times])\mathbf{A}_b^r$. Observed and reference unit vectors are related by $\mathbf{u} = \mathbf{A}(\mathbf{a}_j)\mathbf{A}_b^r\mathbf{A}_i^b(t)\mathbf{u}'$ and substituting

$$\mathbf{u} = \mathbf{A}_b^r\mathbf{A}_i^b(t)\mathbf{u}' - \left[\mathbf{a}_j\times\right]\mathbf{A}_b^r\mathbf{A}_i^b(t)\mathbf{u}' \tag{21}$$

$$\mathbf{u} = \mathbf{A}_b^r\mathbf{A}_i^b(t)\mathbf{u}' + \left[\mathbf{A}_b^r\mathbf{A}_i^b(t)\mathbf{u}'\times\right]\mathbf{a}_j \tag{22}$$

$$\partial\mathbf{u}/\partial\mathbf{a}_j = \left[\mathbf{A}_b^j\mathbf{A}_i^b(t)\mathbf{u}'\times\right] \tag{23}$$

for $\mathbf{a}_b^r \to \mathbf{a}_b^j$ as $\mathbf{a}_j \to \mathbf{0}$.

After propagation of the state and covariance from t_k to t_{k+1} the measurement update at t_{k+1} is performed using the Kalman gain $\mathbf{K} = \mathbf{P}\mathbf{H}^T(\mathbf{H}\mathbf{P}\mathbf{H}^T + \mathbf{R})^{-1}$, estimated state correction

$$\Delta\hat{\mathbf{x}} = \left[\Delta\hat{\mathbf{a}}^T \quad \Delta\hat{\mathbf{b}}^T \quad \Delta\hat{\mathbf{a}}_{LRS}^T \quad \Delta\hat{\mathbf{a}}_{SST1}^T \quad \Delta\hat{\mathbf{a}}_{SST2}^T\right]^T = \mathbf{K}\Delta\mathbf{y} \tag{24}$$

and covariance update $\mathbf{P}_+ = (\mathbf{I} - \mathbf{KH})\mathbf{P}_-$. The rate bias estimate is updated by $\hat{\mathbf{b}}_+ = \hat{\mathbf{b}}_- + \Delta\hat{\mathbf{b}}$, and the attitude error estimate is moved into the reference attitude $\mathbf{q}_{\text{ref}+} = \mathbf{q}(\Delta\hat{\mathbf{a}}) \otimes \mathbf{q}_{\text{ref}-}$. The sensor alignments are updated by $\hat{\mathbf{a}}_{LRS+} = \hat{\mathbf{a}}_{LRS-} + \Delta\hat{\mathbf{a}}_{LRS}$, $\hat{\mathbf{a}}_{SST1+} = \hat{\mathbf{a}}_{SST1-} + \Delta\hat{\mathbf{a}}_{SST1}$, and $\hat{\mathbf{a}}_{SST2+} = \hat{\mathbf{a}}_{SST2-} + \Delta\hat{\mathbf{a}}_{SST2}$.

In this study, only the LRS star tracker alignment is estimated, by holding the SST alignments constant. If there are enough observations, all three trackers' alignments can be observed as described above.

Alignment Tracking Error

LRS alignment error is tracked using the difference between the estimate $\hat{\mathbf{a}}_{LRS}$ and simulated truth $\mathbf{a}_{LRS}$. Quantifying this error[3] starts with performing 1400 runs for each Monte Carlo simulation case, and sampling roll and pitch alignment results every 10 seconds (at 10 Hz, this means 100 state estimates are used for each sample j). Yaw is not considered because star observations are less sensitive to yaw than roll and pitch, and laser pointing accuracy is also less affected by yaw than roll and pitch.

If the vector error for time t_k is $\mathbf{e}(t_k) = \hat{\mathbf{a}}_{LRS}(t_k) - \mathbf{a}_{LRS}(t_k)$ and if $e_k(t_k)$ is the roll or pitch error for the kth state within the 100 used to make sample j, then the mean, rms and standard deviation of roll (or pitch) alignment error for sample j in run i are

$$\mu(i,j) \equiv \sum_{k=1}^{100} e_k(i,j)/100 \tag{25}$$

$$\text{rms}(i,j)^2 \equiv \sum_{k=1}^{100} e_k(i,j)^2/100 \tag{26}$$

$$\sigma(i,j)^2 = \text{rms}(i,j)^2 - \mu(i,j)^2 \tag{27}$$

For all samples in a particular run (to see overall performance for a specific instance, say a given right ascension where there are fewer stars in the sky),

$$\mu(i) = \sum_{j=1}^{n} \mu(i,j)/n \tag{28}$$

$$\text{rms}(i)^2 = \sum_{j=1}^{n} \text{rms}(i,j)^2/n \tag{29}$$

$$\sigma(i)^2 = \text{rms}(i)^2 - \mu(i)^2 \tag{30}$$

Where n is the number of samples over a run (one run is one orbit, or 5670 seconds).

And for all samples over all runs, to evaluate performance for a particular case (one of the nine configurations of sun shade and sensitivity),

$$\mu = \sum_{j=1}^{m} \sum_{i=1}^{n} \mu(i,j)/mn \tag{31}$$

$$\text{rms}^2 = \sum_{j=1}^{m} \sum_{i=1}^{n} \text{rms}(i,j)^2/mn \tag{32}$$

$$\sigma^2 = \text{rms}^2 - \mu^2 \tag{33}$$

Performance Statistics

Sunshade performance is characterized using sets of orbits with similar minimum sun angles, or similar nearest approaches to the sun. The orbits within a set have random ascending nodes, and for large sets the LRS effectively observes the full sky. Orbits are grouped here into 7 sets or bins from 0° to 70°, with minimum sun angles ranging over 10° within each bin.

Performance is evaluated separately in each of the 7 bins for a histogram covering the range from very near the sun to relatively distant from the sun. Statistics are computed within each bin to reflect the uncertainties in pointing knowledge when the sun angle is less than 90°, so in daylight. Results from the night side of each orbit are not included since they are not affected by the sunshade.

For each orbit, a 10 Hz time series of roll and pitch errors are produced by the processor. A subsampling of this output is performed immediately to reduce computation demands. The values stored for post-processing analysis are the sums $a \equiv \sum x_k$ and $b \equiv \sum x_k^2$ for subsamples covering 10 seconds. For subsample i, the mean error is $a_i/100$, the rms error is $\sqrt{b_i^2/100}$, and the error variance is $c_i^2 \equiv b_i^2/100 - (a_i/100)^2$.

Within a bin, the subsample values and from all orbits are accumulated as two vectors. For a bin containing m orbits and n daylight subsamples per orbit, $i = 1,\ldots,mn$. Significant parameters used in the results section are the mean rms error within a bin,

$$\text{mean rms error within a bin} = \left(\sum_{i=1}^{mn} \sqrt{b_i^2/100} \right) \tag{34}$$

And the standard deviation of the mean,

$$\text{standard deviation of the mean} = \left(\sum_{i=1}^{mn} c_i^2 \right)^{1/2} / (mn)^{1/2} \tag{35}$$

Increasing the number of orbits (Monte Carlo runs) m scales the uncertainty of the mean rms error by a factor of $1/\sqrt{m}$.

RESULTS

To characterize the performance of the LRS, 1400 orbits are run in each of the nine cases, and the distribution of the orbits by closest approach to sun is random between 0° and 70°, so each case contains approximately 200 runs per bin. The two bounding cases from the nine LRS sensitivity curves (Figure 5) characterize the range of expected performance results. The best-case scenario combines LRS sensitivity 6.0 with sunshade degraded zone outer radius 40°. The worst case combines sensitivity 5.0 with outer radius 60°.

Figure 6 is a representation of the results of a particular orbit showing two cases: one with a base star sensor sensitivity of 5.0 (worse) and the other with 5.5 (better). In both cases, the sun shade is the same: the worst case where the sun starts affecting the sensor from 60° inwards (vertical dotted lines). The figure presents quite a few features: it shows sun blinding near 0 degrees; a decrease in the number of stars as sun angle goes from 60° to 20°, reaching complete blindness inside the 20° radius (vertical dashed lines) around the LRS-zenith. A star gap in the sky is also visible on the left side of Figure 6, where the number of stars reaches zero outside the blinding

zone. The gap is shorter for the better 5.5 case (green) than the 5.0 case (blue), simply because the sensor with sensitivity 5.5 sees more, and dimmer stars.

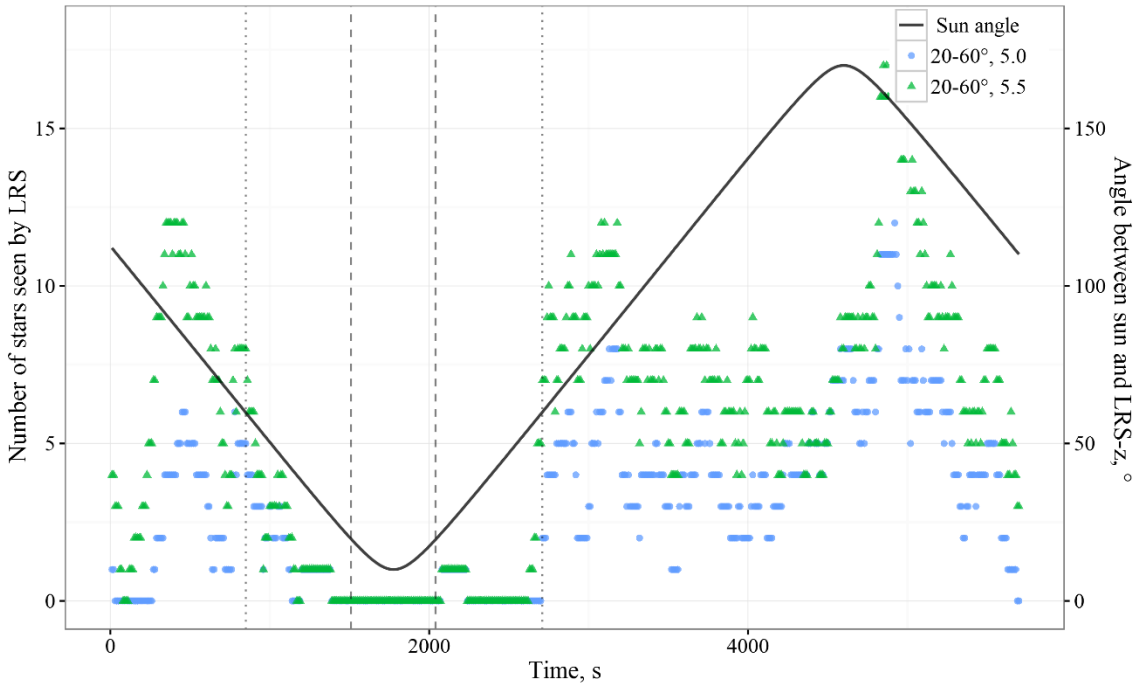

Figure 6. Number of LRS stars visible in a particular run

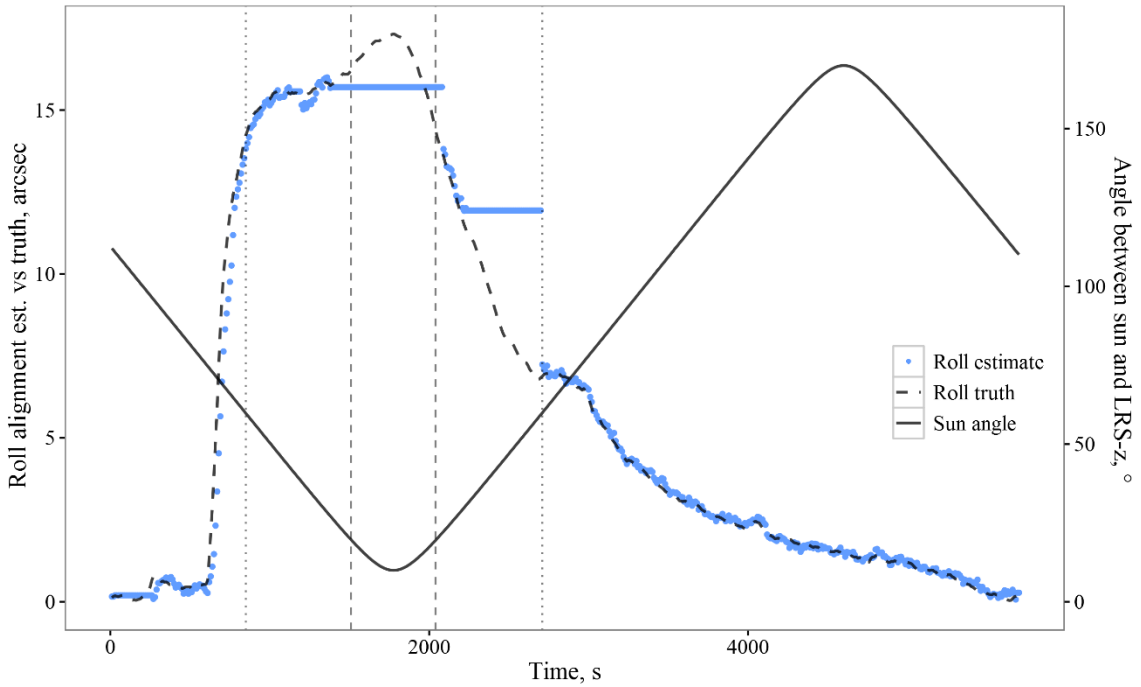

Figure 7. LRS roll alignment estimate for a particular run

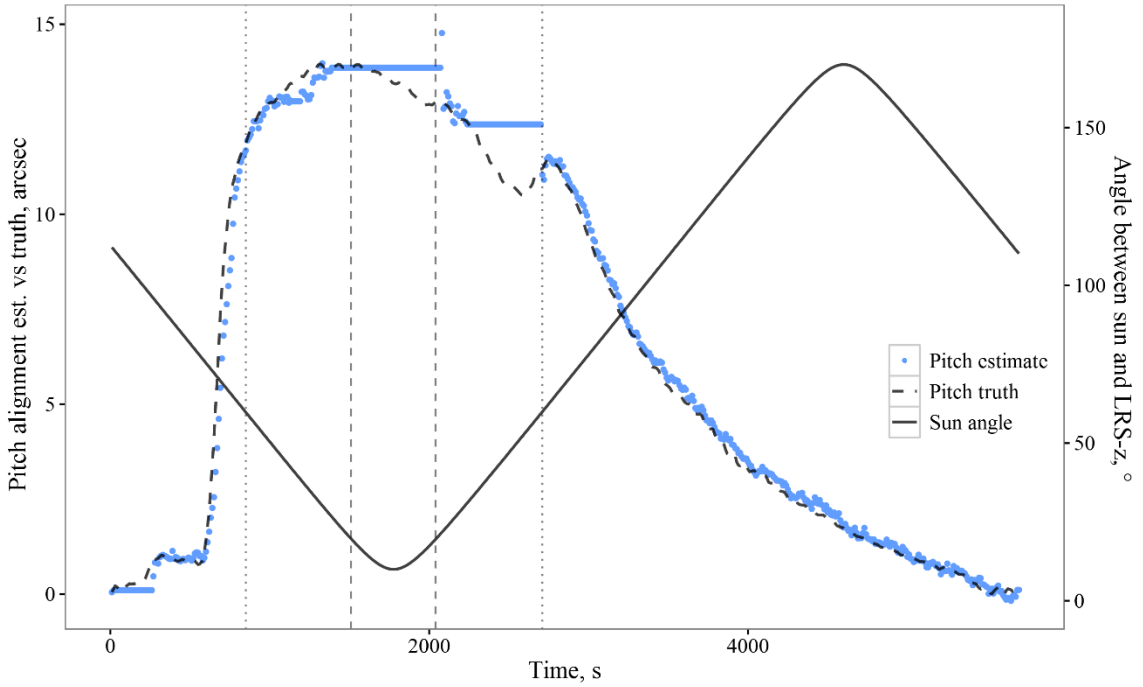

Figure 8. LRS pitch alignment estimate for a particular run

Figure 7 and Figure 8 show roll and pitch alignment estimates respectively over a complete orbit for the same run represented in Figure 6, so the correlation between number of sun blinding / star gaps and alignment estimates can be seen. When no star information is available, there is no alignment output from the LRS, and the filter assumes the change in alignment is zero, resulting in the flat lines in Figure 7 and Figure 8. The sun blinding / star gaps are the same length in both roll and pitch estimates, but slopes of the pitch alignment are much shallower, so accumulated error is smaller than roll (compare Figure 9 and Figure 10 to see this difference).

Figure 9 and Figure 10 show the mean rms errors in roll and pitch, and standard deviations of the means, Equation (34) and Equation (35), for the bounding cases and a middle, expected case. Performance differs by approximately a factor of two between the extreme cases, and pitch performance is approximately a factor of two better than roll performance.

Away from the Sun, performance approaches a steady state with rms errors of approximately 0.2 to 0.4 arcseconds. This is what the pointing knowledge would be if there were no sun blinding. The roll results are worse than pitch simply because the roll and pitch alignment inputs are different, with roll being steeper than pitch, so that the alignment during sun blinding / star gaps is further from the truth in the roll case than the pitch case. Figure 11 shows the average number of stars visible in the LRS field-of-view (FOV) in each case. There is a strong correlation between the number of visible stars and alignment performance, as expected.

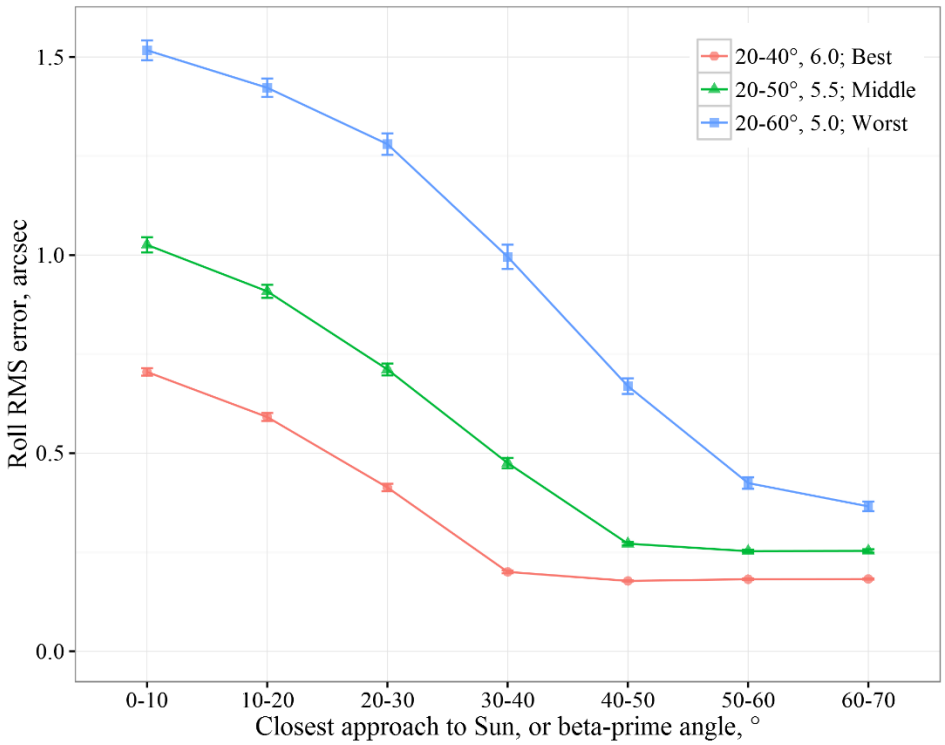

Figure 9. Binned roll alignment performance results

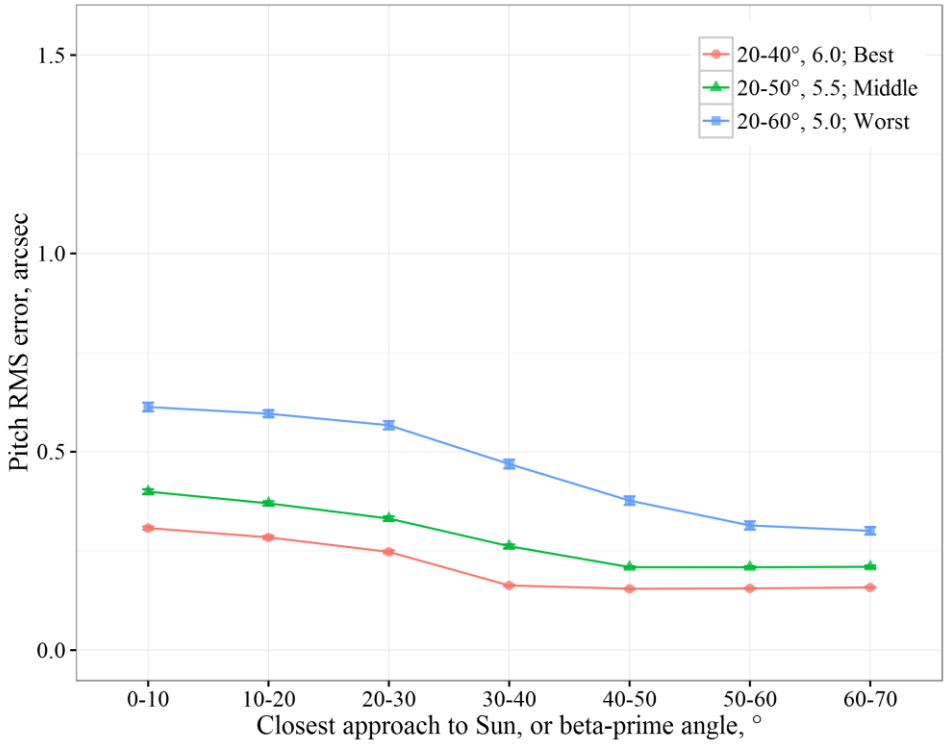

Figure 10. Binned pitch alignment performance results

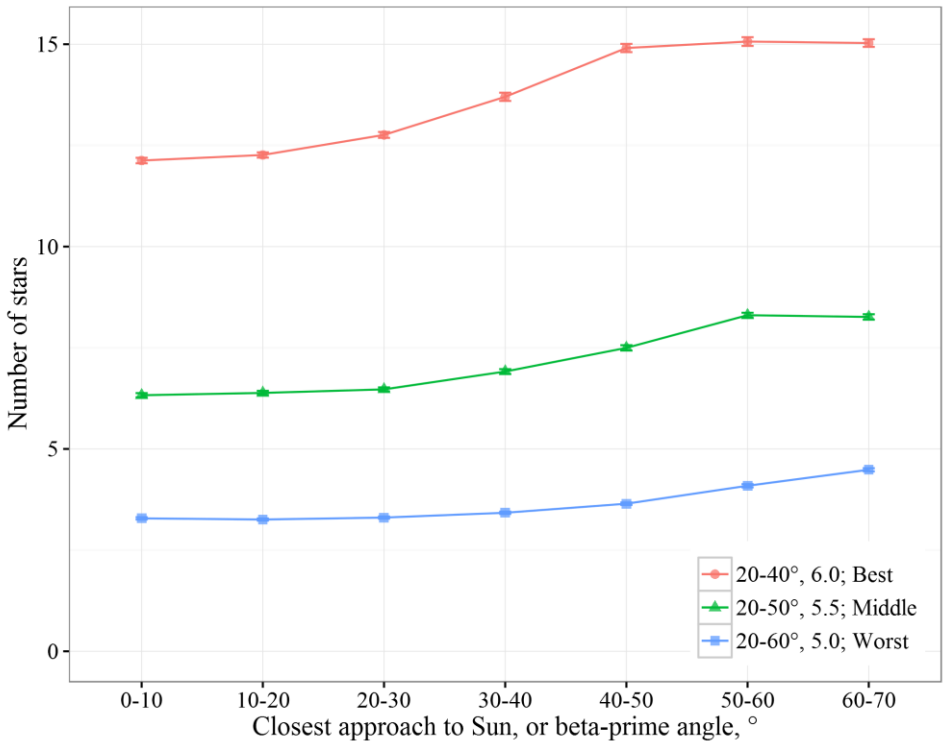

Figure 11. Average number of stars visible in the LRS FOV per case

CONCLUSIONS

There is a quantifiable correlation between the LRS alignment errors and the number of LRS star observations, which, in the vicinity of the sun, goes to zero in all cases (in worse cases, even before the sensitivity reaches 0 in a 20° radius around the sun). Since the motion of the LRS is unknown, and can only be modeled from observations once ICESat-2 is in orbit, we must find ways to mitigate the loss of star data during sun blinding and during regions of the sky when stars are sparse enough that no stars are visible in the star tracker field of view.

The results show that when the sun is at or near the zenith of the LRS star tracker there is significant degradation in performance, and at such times the observations from the spacecraft star trackers (SSTs) can provide a better estimate of the spacecraft attitude (the SSTs cannot be blinded at the same time as the LRS because of their configuration on the spacecraft; see Figure 1).

The LRS star observations are affected by three factors: base star sensor sensitivity (there is a large jump in average number of visible stars when sensitivity is increased from 5.5 to 6.0), sun shade performance (sun blinding gaps are longer for worse sun shades), and star gaps (there are more star gaps when base sensitivity is low). The first two factors are evident in Figure 11: from left to right the effect of the sun shade is apparent, where the best sun shade keeps the sun from affecting star observations from 40° outwards; and from bottom to top the effect of improving the base sensitivity, where the total number of visible stars goes from just 1400 at sensitivity 5.0, to 2456 at 5.5, up to 4376 at 6.0.

ACKNOWLEDGEMENTS

The research conducted in this study was supported by NASA Grant NNX12AI19G.

NOTATION

$\mathbf{A}_i^{ATLAS}$	=	true reference platform attitude
$\mathbf{A}_i^b$	=	estimated reference platform and body frame attitude
$\mathbf{A}_{ATLAS}^{LRS}$	=	constant reference alignment of laser reference sensor
$\mathbf{A}_b^{LRS}$	=	estimated laser reference sensor attitude
$\mathbf{A}_i^{LRS}$	=	true laser reference sensor attitude
$\mathbf{A}_{ATLAS}^{SST}$	=	constant reference alignment of spacecraft star trackers
$\mathbf{A}_i^{SST}$	=	true spacecraft star tracker attitudes
$\mathbf{a}$	=	attitude error rotation vector
$\hat{\mathbf{a}}$	=	estimated attitude error rotation vector
$\mathbf{a}_{LRS}$	=	true alignment rotation vector
$\mathbf{b}$	=	gyro rate bias
$\mathbf{H}$	=	observation sensitivity matrix
$\mathbf{h}(\mathbf{u})$	=	star observation model
$\mathbf{K}$	=	Kalman gain matrix
m	=	instrument and star magnitudes
$\mathbf{P}$	=	state covariance matrix
$\mathbf{Q}$	=	process noise covariance matrix
$\mathbf{q}_b$	=	reference attitude quaternion
$\mathbf{R}$	=	measurement noise covariance matrix
$\mathbf{u}_{obs}$	=	simulated star observation unit vector
$\mathbf{u}_{ref}$	=	star catalog unit vector in ICRF
$\mathbf{x}$	=	state vector
$\hat{\mathbf{x}}$	=	estimated state vector
$\Delta\mathbf{y}$	=	observation residual rotation vector
$\mathbf{\Phi}$	=	state transition matrix
$\boldsymbol{\eta}$	=	zero-mean Gaussian noise vector
$\boldsymbol{\omega}$	=	true angular rate vector, rad/s
$\boldsymbol{\omega}_g$	=	gyro output angular rate vector, rad/s

REFERENCES

[1] Bae, S., Magruder, L., Ricklefs, R., Webb, C., Yoon, S., and Schutz, B. E., "ICESat/GLAS Precision Attitude Determination For Early Laser Operation," Paper AAS 04-118, AAS/AIAA Space Flight Mechanics Meeting, Maui, HI, 2004.

[2] Bae, S. and Schutz, B. E., "Precision Attitude Determination Using Gyro And Star Tracker Data With A Batch Least Squares Estimator," Paper AAS 05-260, AAS/AIAA Astrodynamics Conference, Advances in the Astronautical Sciences, Vol. 123, Univelt, San Diego, CA, 2005, pp. 175-182.

[3] Smith, N., Bae, S., and Schutz, B. E., "Laser Reference Sensor Alignment Tracking And Star Observations," *Journal of Spacecraft and Rockets*, Vol. 51, No. 6, 2014, pp 1836-1848. doi:10.2514/1.A32966

[4] Kaula, W. M., "Satellite Orbit Dynamics", *Theory of Satellite Geodesy: Applications of Satellites to Geodesy*, Dover, New York, 2000, pp. 39

[5] Pittelkau, M. E., "Kalman Filtering For Spacecraft System Alignment Calibration," *Journal of Guidance, Control, and Dynamics*, Vol. 24, No. 6, 2001, pp. 1187-1195. doi: 10.2514/2.4834

[6] Pittelkau, M. E., "Everything Is Relative In Spacecraft System Alignment Calibration," *Journal of Spacecraft and Rockets*, Vol. 39, No. 3, 2002, pp. 460-466. doi: 10.2514/2.3830

[7] Markley, F. L., "Attitude Error Representation For Kalman Filtering," *Journal of Guidance, Control, and Dynamics*, Vol. 26, No. 2, 2003, pp. 311-317. doi: 10.2514/2.5048

[8] Smith, N., Bae, S., and Schutz, B. E., "Biased Star Tracker Measurements Of Forty-Nine Stars From Flight Data," *Journal of Spacecraft and Rockets*, Vol. 47, No. 6, 2010, pp. 1023-1028. doi: 10.2514/1.49412